

Falsifiability Test for Classical Nucleation Theory

Camilla Beneduce¹, Diogo E. P. Pinto¹, Lorenzo Rovigatti¹, Flavio Romano²,

Petr Šulc^{3,4,5}, Francesco Sciortino¹, and John Russo¹

¹*Dipartimento di Fisica, Sapienza Università di Roma, P.le Aldo Moro 5, 00185 Rome, Italy*

²*Department of Molecular Sciences and Nanosystems, Ca' Foscari University of Venice, Via Torino 155, 30171 Venezia-Mestre, Italy*

³*School of Molecular Sciences and Center for Molecular Design and Biomimetics, The Biodesign Institute, Arizona State University, 1001 South McAllister Avenue, Tempe, Arizona 85281, USA*

⁴*Center for Biological Physics, Arizona State University, Tempe, Arizona 85281, USA*

⁵*TU Munich, School of Natural Sciences, Department of Bioscience, Garching, Germany*



(Received 16 September 2024; revised 18 December 2024; accepted 3 March 2025; published 7 April 2025)

Classical nucleation theory (CNT) is built upon the capillarity approximation, i.e., the assumption that the nucleation properties can be inferred from the bulk properties of the melt and the crystal. Although the simplicity and usefulness of CNT cannot be overstated, experiments and simulations regularly uncover significant deviations from its predictions, which are often reconciled through phenomenological extensions of the CNT, fueling the debate over the general validity of the theory. In this Letter, we present a falsifiability test for any nucleation theory grounded in the capillarity approximation. We focus on cases where the theory predicts no differences in nucleation rates between different crystal polymorphs. We then introduce a system in which all polymorphs have the same free energy (both bulk and interfacial) across all state points. Through extensive molecular simulations, we show that the polymorphs exhibit remarkably different nucleation properties, directly contradicting predictions of CNT. We argue that CNT's primary limitation lies in its neglect of structural fluctuations within the liquid phase.

DOI: [10.1103/PhysRevLett.134.148201](https://doi.org/10.1103/PhysRevLett.134.148201)

Citing Peters (who in turn paraphrases Popper [1]): “The most convincing test of a theory comes from special cases where the theory should fail if it is not true” [2]. Here, we present a system that is ideally suited to test one of the basic assumptions of classical nucleation theory (CNT), i.e., the so-called *capillarity approximation*. The capillarity approximation assumes that the critical nucleus has the same thermodynamic properties (surface tension, density, etc.) of the bulk phase, which allows for a simple calculation of the free-energy barrier for the phase transition. CNT defines the nucleation rate as $K e^{-\Delta G(n_c)/k_B T}$, where $k_B T$ is the thermal energy, and K is the kinetic prefactor that accounts for the attachment rate of particles to the nucleus. $\Delta G(n_c)$ is the free-energy barrier for nucleation and is obtained by maximizing $\Delta G(n) = -n|\Delta\mu| + \alpha n^{2/3}\gamma$, i.e., the Gibbs free energy cost to form a nucleus of n particles at constant pressure and temperature, where $\Delta\mu$ is the chemical potential difference between the crystal and the melt, γ is the interfacial free energy, and α is a proportionality constant accounting for the shape of the nucleus [3]. Because of its relative simplicity and predictive power, CNT has been perhaps the most used theoretical model to describe nucleation processes. Although it has been successful in many cases [4–7], there are also numerous cases where its predictions do not align with experimental and simulation results [8–11]. In such instances, various phenomenological

extensions to the theory [12–26] have been proposed to reconcile these discrepancies without abandoning the capillarity approximation, for example, by introducing temperature-dependent interfacial free energies.

Usual tests of CNT consist in comparing the measured nucleation rates with theoretical values. The problem with this approach is that the results depend strongly on quantities, notably γ , which are state dependent and very difficult to measure accurately at conditions where homogeneous nucleation occurs. Citing Oxtoby, “Nucleation theory is one of the few areas of science in which agreement of predicted and measured rates to within several orders of magnitude is considered a major success” [27].

Here we present a falsifiability test not only for CNT but also for any nucleation theory grounded in the capillarity approximation. Instead of accurately predicting nucleation rates, we focus on the polymorphic composition of the crystalline phase [28,29], i.e., the ability of a material to exist in more than one crystalline structure [30–36]. We introduce a binary mixture with three polymorphs that possess identical free energies (both bulk and interfacial) at all state points. The three polymorphs are isotypic forms of the cubic diamond crystal, i.e., they share the same atomic positions and symmetry of the crystal lattice, but differ in the way the different species are arranged on the lattice sites. Within the capillarity approximation all these structures should have identical nucleation properties, given that there

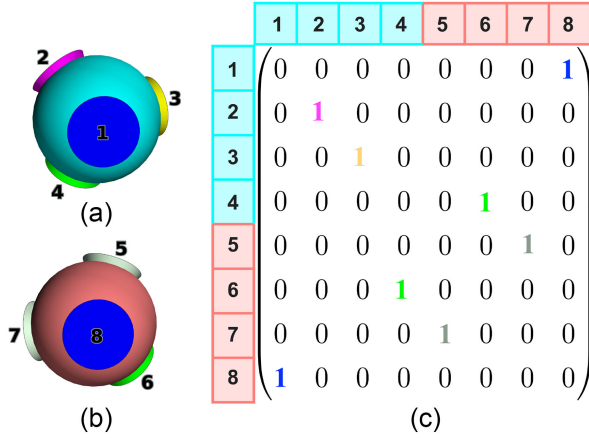


FIG. 1. N2c8 design. Binary mixture of patchy particles SAT-designed to exclusively self-assemble into a cubic diamond crystal. The two species, depicted in cyan (a) and red (b), have four tetrahedrally arranged patches that bind according to the interaction matrix (c) where the ones indicate the interacting patches. Matching colors appear for complementary patches (off-diagonal ones), while unique colors represent self-complementary interactions (diagonal ones).

are no free-energy differences between the different polymorphs and that they all form from the same liquid phase. Instead, via molecular simulations, we find that the nucleation properties of the three polymorphs are radically different. Interestingly, we find that the polymorph that nucleates more easily is the one with the largest unit cell, and the one that nucleates the least is the one with the smallest unit cell. To account for the difference in nucleation properties between the polymorphs, we show that the orientational order of the melt is closest to the polymorph that nucleates more frequently.

The model system is presented in Fig. 1. It is a binary mixture of tetravalent patchy particles, i.e., particles that have a hard-core repulsion and attractive spots tetrahedrally located on their surface, as detailed in Supplemental Material [37]. The interaction between the patches is specific and defined by the interaction matrix in Fig. 1(c), whose

elements m_{ij} are equal to 1 only if patches i and j can bind. The specificity of interactions in patchy particles model systems can be experimentally realized exploiting the predictable and controllable interactions (Watson-Crick base pairing) of DNA [44–46], with one of the most promising approaches being the use of DNA origami [47,48]. This technique has recently been successfully applied to the self-assembly of a pyrochlore lattice, confirming the feasibility of the approach [49]. The design in Fig. 1, called N2c8, since it uses two species and eight different patch types, was originally introduced in the context of SAT assembly [50,51] as a system able to self-assemble exclusively into the cubic diamond structure (DC) while avoiding the hexagonal diamond one [52]. As explained in the dedicated section in Supplemental Material [37], the SAT-assembly algorithm can also be used to list all possible ways to fill the lattice positions of the target cell by particles belonging to a selected design (in our case N2c8). This allows us to automatically identify all those possible polymorphs that, regardless of their nucleation abilities, are compatible with a cubic diamond lattice of a certain size (defying McCrone’s law [53]). We find that there are three possible periodically repeated patterns of N2c8 patchy particles within the lattice positions of a 48-particle cubic diamond cell. All these arrangements are illustrated in Fig. 2 where we display the [001] plane. The three structures belong to the P1 space group, meaning that there is no symmetry other than the translational one. Yet, they differ in the unit cell size (black box in Fig. 2), which we use for labeling: DC-X where $X \in [8, 16, 24]$ refers to the size of the unit cell of each polymorph. We use here the word unit cell to indicate the smallest repeating unit of the two species, regardless of patch coloring, that, when stacked together, creates the crystal lattice, as shown in Fig. 2. It is worth noting that if the patch arrangement in the unit cell is also considered (not shown in Fig. 2), the DC-8, DC-16, DC-24 have unit cells of 16, 16, and 48 atoms, respectively. In the following, we will indicate the size of the unit cell only referring to the species occupation, regardless of the patch arrangement. Although

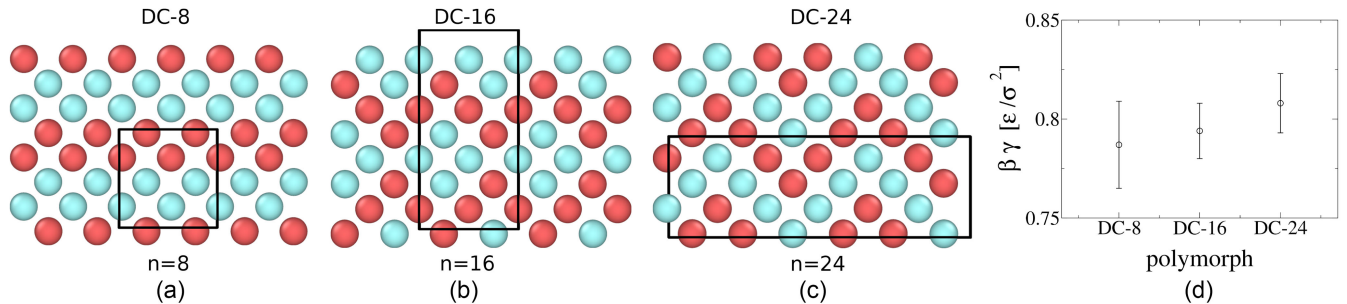


FIG. 2. Overview of cubic diamond polymorphs. The SAT-assembly framework allows us to enumerate all the possible arrangements of the N2c8 particles in the 48 particle cubic diamond lattice. Three periodic patterns are identified: DC-8 (a), DC-16 (b), and DC-24 (c). They are labeled and displayed in increasing order of unit cell size (black box). In (d) their surface tensions are plotted. Each estimate comes from an average of four independent Monte Carlo simulations in the grand canonical ensemble. All values are considered equal within an error of 3%.

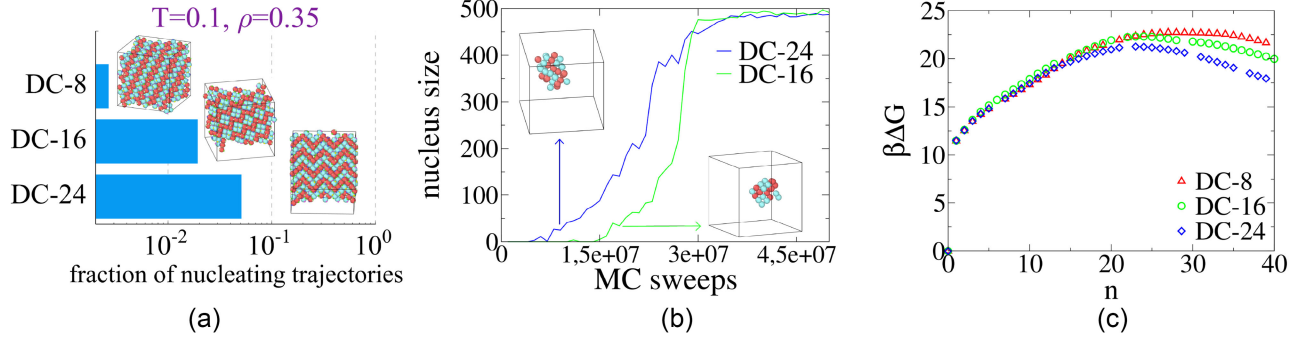


FIG. 3. Direct nucleation simulations and nucleation barriers (a) Fraction of trajectories ending up into each polymorph out of 600 with snapshots of final configurations. Simulations are run in the canonical ensemble at $T = 0.1, \rho = 0.35, N = 500$. Interestingly, the polymorph with the largest unit cell size is the one that nucleates most frequently. (b) Time evolution of the number of crystalline particles with a snapshot of the critical nucleus for the DC-24 (blue) and the DC-16 (green) structures. (c) Gibbs free energy for the formation of crystal nucleus of size n for the three polymorphs computed by means of umbrella sampling technique at $T = 0.104$ and $P = 0.018$. The different trend in nucleation simulations is confirmed: the smallest unit cell size polymorph has the highest barrier.

other polymorphs with larger unit cell sizes exist, they do not appear in our simulations because nucleation involves critical nuclei smaller than 30 particles under the conditions investigated. We speculate that crystals with unit cells larger than the critical nucleus size n_c , which is temperature dependent, are prevented from nucleating.

The three polymorphs investigated here are isotypic, their composition is always equimolar and they have only translational symmetry. In each of the crystals the same number and type of bonds are established, and lattice vibrations are controlled by the geometry of the patches, which is the same for both species of the mixture. Therefore, all polymorphs have the same bulk free energy. Moreover, we verify the equality of their (solid-liquid) interfacial free energies. With successive umbrella sampling simulations [54] we have computed the free energy cost of forming an interface between each polymorph and the same liquid phase at coexistence conditions (determined via direct coexistence simulations). The resulting average values of surface free energy are reported in Fig. 2(d) for the [100] square plane. We leave the full description on how the computation is performed in the dedicated section of the Supplemental Material [37]. Here we just emphasize that the surface tensions of the three polymorphs are the same within the error (approximately 3%). The relevant macroscopic properties on which CNT is based are therefore the same in the DC-8, the DC-16, and the DC-24 structures.

Having characterized the bulk properties of the three polymorphs, we now consider their nucleation properties. The N2c8 binary mixture has an azeotropic point at equimolar concentration [55], meaning that an equimolar mixture will retain its composition during liquid-gas phase separation. This was shown to aid the nucleation process [56], since crystal nucleation can occur in liquid droplets that have the same composition as the final crystalline structure. We choose two state points where crystallization was found to be favorable and we run extensive

Monte Carlo simulations in the canonical ensemble to collect nucleation events. In the following, temperature T is in unit of ϵ/k_B , density ρ is in unit of $1/\sigma^3$, and pressure P in unit of ϵ/σ^3 , where σ is the patchy particle diameter, ϵ is the square-well potential depth (see Supplemental Material [37]) and $k_B = 1$. In particular, we simulate $N = 500$ patchy particles [57] at equimolar concentration in the canonical ensemble at $T = 0.1, \rho = 0.35$ [600 trajectories, both with and without aggregation-volume bias (AVB) moves [57,58]] and at $T = 0.104, \rho = 0.4$ (300 trajectories with AVB dynamics). We label successfully nucleated those trajectories having a fraction of particles in the cubic diamond phase greater than 0.5 and classify the obtained crystals. We use the total coherence, an order parameter based on spherical harmonics, to distinguish between liquid and crystalline particles [59–62], and we implement a new order parameter (bond geometry and particle orientations must be taken into account) to classify the different polymorphs. A full description of the order parameters can be found in the section “Total coherence order parameter” in the Supplemental Material [37]. As shown in Fig. 3(a), the three polymorphs have different nucleation rates: the majority of nucleating trajectories form the DC-24 polymorph, the one with the largest unit cell size, while only a single nucleation event is observed for the one with the smallest unit cell size, the DC-8 polymorph. Specifically, for the $T = 0.1, \rho = 0.35$ state point, out of 600 trajectories, 43 form the DC-24, 15 the DC-16, and none the DC-8 with AVB dynamics and 30 form the DC-24, 11 the DC-16, and 1 the DC-8 with no AVB moves. Similar results are observed for the $T = 0.104, \rho = 0.4$ state point (35, 6, and 0, respectively, out of 300 trajectories). In Fig. 3(b) we report the progress in time of the nucleus size for two typical trajectories: the blue one spontaneously self-assembling a DC-24 polymorph, and the green one crystallizing into a DC-16 structure. Snapshots of the critical nucleus are also displayed, showing that the different polymorphs are already distinguishable at

critical sizes. Additionally, we analyze the polymorph growth (see Supplemental Material [37]) to explicitly exclude the presence of cross nucleation of one polymorph on top of another.

The different nucleation rates of the three polymorphs are reflected by the height of their free energy barriers, which we compute with the umbrella sampling technique (a brief description is provided in the Supplemental Material [37]). For this, we run *NPT* Monte Carlo simulations at $T = 0.104$ and $P = 0.018$ with a harmonic bias potential. Each simulation is prepared by inserting in the liquid phase a crystalline seed of size n_0 , where n_0 increases by 5 particles in successive simulations. The initial seeds have a roughly spherical shape and the same density for each polymorph. We carefully verify that the chosen bias potential and thermodynamic conditions ensure a good sampling, i.e., that there is an appreciable overlap between simulations with successive n_0 , that no spontaneous nucleation occurs, and that there is no change in polymorph identity during the simulation. The resulting barriers are reported in Fig. 3(c). In order of increasing barrier height, we find DC-24, then DC-16, and finally DC-8, confirming that the polymorph with the lowest barrier is the one with the largest unit cell. The height difference between the DC-24 and DC-16 barrier is approximately $1k_B T$, a value that aligns well with the fractions of trajectories nucleating into the two polymorphs. The same comparison cannot be made for the DC-8 case as only a single nucleation event is observed for this polymorph. The critical size n_c for all nuclei is $n_c \lesssim 30$, i.e., smaller than the largest unit cell (48 particles) used in our exhaustive search of competing polymorphs.

We have observed that the three polymorphs exhibit different nucleation properties, specifically in terms of nucleation rates and barrier heights, and that these differences cannot be attributed to variations in the bulk properties of the crystals. In the following, we investigate whether the different nucleation properties of the polymorphs can instead be traced back to the structural fluctuations within the melt. We follow the idea that if the liquid phase from which the nucleus arises already exhibits some degree of order in particle orientation, this will favor the nucleation of the polymorph that is structurally closer to the melt [63]. The three polymorphs, DC-8, DC-16, and DC-24, differ in fact by the orientation between neighbors of the same species. In particular, for each patchy particle, we can consider the angle α formed between the patch orientations of its two second-nearest neighbor of the same species [see inset of Fig. 4(b)]: for the bulk polymorphs we have $\alpha_{\text{DC-24}} \sim 109^\circ$, $\alpha_{\text{DC-16}} \sim 9^\circ$, and $\alpha_{\text{DC-8}} \sim 9^\circ$. In Fig. 4(b) we plot the radial profile of α from the center of mass of nuclei of DC-24 (blue diamonds), DC-16 (green circles), and DC-8 (red triangles) polymorphs. We use configurations and trajectories from the umbrella sampling window of size $n \sim 50$ and, in order to compute α , we consider only particles having two second nearest neighbors of the same species. To show the crystalline

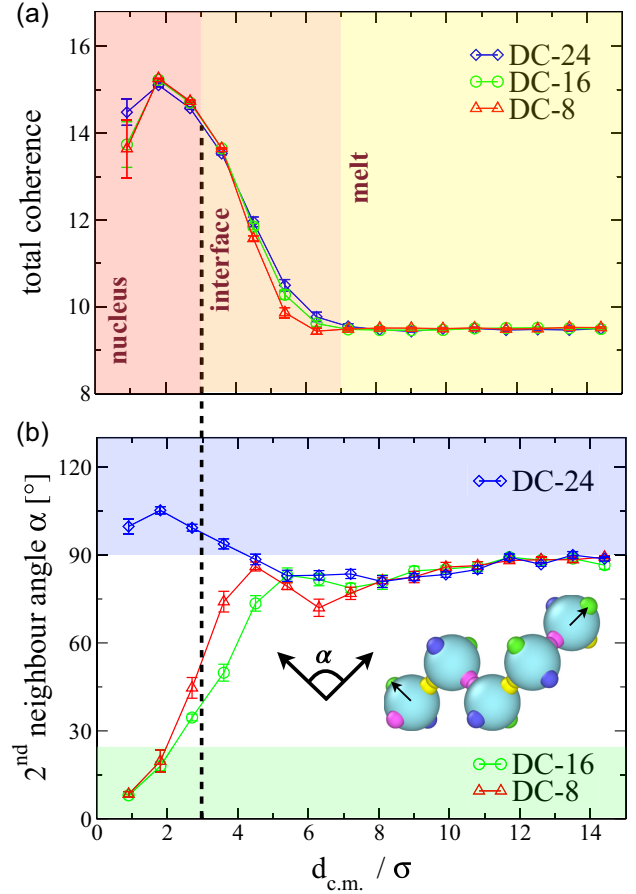


FIG. 4. Bond orientational order in the liquid phase. Total coherence (a) and α angle (b) as a function of the distance of each particle from the center of mass $d_{\text{c.m.}}$ of the largest crystalline cluster. Points are computed by averaging on different configurations and trajectories characterized by a crystalline nucleus of 50 particles: a DC-24 (blue diamonds), a DC-16 (green circles), and a DC-8 (red triangles) nucleus. α defines the relative orientation between second neighbors of the same species as illustrated for patchy particles of the first species of the DC-24 polymorph in the inset of (b). The colored bands in (a) help locating the different regions: the nucleus, the interface, and the melt. The colored bands in (b) define the range of α values typical of the bulk DC-24 crystal (blue band) and of the bulk of both DC-16 and DC-8 (green band) polymorphs; particles in the interfacial region as well as the ones in the melt have α angles characteristic of the DC-24 structure.

profile, in Fig. 4(a), we show the radial distribution of the total coherence which has high values (around 14) for the bulk diamond crystal, and small values (around 9.5) for the melt, irrespective of the polymorph. The figure shows the transition from the core of the nuclei at short distances to the melt at large distances. In the core region, α assumes the value of the corresponding bulk polymorph ($\alpha_{\text{DC-24}} \sim 109^\circ$, $\alpha_{\text{DC-16}} \sim 9^\circ$, and $\alpha_{\text{DC-8}} \sim 9^\circ$). In the interfacial region, instead, the value of α is always that of DC-24 polymorph, irrespectively, of the nucleus type. This shows that the orientational order in the melt resembles more closely that

of the DC-24 polymorph, i.e., the polymorph which nucleates more frequently and has the lowest nucleation barrier. A similar argument can be made to rationalize why the DC-8 is the less frequently nucleating polymorph, as discussed in the Supplemental Material [37]. Furthermore, a thorough analysis confirms that the observed difference in the nucleation frequency between the polymorphs cannot be attributed to the presence of favorable or unfavorable bonding sites on their surfaces (see Supplemental Material [37]).

In conclusion, unlike previous tests of classical nucleation theory, which focus on accurately measuring nucleation rates and comparing them to theoretical predictions, leading to a pass or fail outcome depending on the system and/or state point, in this Letter we propose an alternative approach. We examine cases where CNT predicts no difference in nucleation rates between different polymorphs. This shift in focus sidesteps the common reliance on precise free-energy measurements and their dependence on specific state points. Instead, it only requires ranking the polymorphs according to their nucleation frequency. Crucially, while discrepancies between CNT and measured nucleation rates can often be accounted for through *ad hoc* extensions to the theory, our test cannot be satisfied by any modification of CNT built upon the capillarity approximation. To run the falsifiability test we introduce a binary mixture of patchy particles where three different polymorphs, despite having identical bulk and interfacial free energies, exhibit significantly different nucleation rates.

One of the shortcomings of CNT is its failure in accounting for the short-range order possessed by the supercooled liquid state [63]. In our system, we have shown that the melt exhibits a local orientational order typical of the polymorph with the highest nucleation rate. This suggests that it is the structural fluctuations in the melt, both in terms of their size and orientational order, rather than the bulk properties of the infinitely large crystals, that determine which polymorph will nucleate. These arguments offer support to approaches beyond CNT that take into account the structural properties of the liquid phase [30,63–73].

Acknowledgments—C. B., D. P., L. R., F. S., and J. R. acknowledge support by ICSC–Centro Nazionale di Ricerca in High Performance Computing, Big Data and Quantum Computing, funded by European Union–NextGenerationEU, and CINECA-ISCRA for HPC resources. D. P. and F. S. acknowledge support from MIUR-PRIN Grant No. 2022JWAF7Y. Work by P. Š. was supported by the U.S. Department of Energy (DOE), Office of Science, Basic Energy Sciences (BES) under Award No. DE-SC0025265.

[1] K. Popper, *Conjectures and Refutations* (Harper and Row, New York, 1963).

[2] B. Peters, Crystal nucleation: Rare made common and captured by raman, *Proc. Natl. Acad. Sci. U.S.A.* **119**, e2204971119 (2022).

- [3] K. Kelton and A. L. Greer, *Nucleation in Condensed Matter: Applications in Materials and Biology* (Elsevier, New York, 2010).
- [4] R. C. Miller, R. J. Anderson, J. Kassner Jr, and D. E. Hagen, Homogeneous nucleation rate measurements for water over a wide range of temperature and nucleation rate, *J. Chem. Phys.* **78**, 3204 (1983).
- [5] R. Strey, P. Wagner, and Y. Viisanen, The problem of measuring homogeneous nucleation rates and the molecular contents of nuclei: Progress in the form of nucleation pulse measurements, *J. Phys. Chem.* **98**, 7748 (1994).
- [6] A. A. Manka, D. Brus, A.-P. Hyvärinen, H. Lihavainen, J. Wölk, and R. Strey, Homogeneous water nucleation in a laminar flow diffusion chamber, *J. Chem. Phys.* **132**, 244505 (2010).
- [7] S. C. C. Prado, J. P. Rino, and E. D. Zanotto, Successful test of the classical nucleation theory by molecular dynamic simulations of bas, *Comput. Mater. Sci.* **161**, 99 (2019).
- [8] H. Lihavainen, Y. Viisanen, and M. Kulmala, Homogeneous nucleation of n-pentanol in a laminar flow diffusion chamber, *J. Chem. Phys.* **114**, 10031 (2001).
- [9] T. H. Zhang and X. Y. Liu, How does a transient amorphous precursor template crystallization, *J. Am. Chem. Soc.* **129**, 13520 (2007).
- [10] K. Iland, J. Wölk, R. Strey, and D. Kashchiev, Argon nucleation in a cryogenic nucleation pulse chamber, *J. Chem. Phys.* **127**, 154506(2007).
- [11] D. Erdemir, A. Y. Lee, and A. S. Myerson, Nucleation of crystals from solution: Classical and two-step models, *Acc. Chem. Res.* **42**, 621 (2009).
- [12] R. C. Tolman, The effect of droplet size on surface tension, *J. Chem. Phys.* **17**, 333 (1949).
- [13] J. Langer, Theory of nucleation rates, *Phys. Rev. Lett.* **21**, 973 (1968).
- [14] M. Plischke and Z. Rácz, Active zone of growing clusters: Diffusion-limited aggregation and the Eden model, *Phys. Rev. Lett.* **53**, 415 (1984).
- [15] P. A. Rikvold, H. Tomita, S. Miyashita, and S. W. Sides, Metastable lifetimes in a kinetic Ising model: Dependence on field and system size, *Phys. Rev. E* **49**, 5080 (1994).
- [16] I. Ford, Nucleation theorems, the statistical mechanics of molecular clusters, and a revision of classical nucleation theory, *Phys. Rev. E* **56**, 5615 (1997).
- [17] R. A. Ramos, P. A. Rikvold, and M. A. Novotny, Test of the Kolmogorov-Johnson-Mehl-Avrami picture of metastable decay in a model with microscopic dynamics, *Phys. Rev. B* **59**, 9053 (1999).
- [18] S. W. Sides, P. A. Rikvold, and M. A. Novotny, Kinetic Ising model in an oscillating field: Avrami theory for the hysteretic response and finite-size scaling for the dynamic phase transition, *Phys. Rev. E* **59**, 2710 (1999).
- [19] D. Reguera and H. Reiss, Extended modified liquid drop-dynamical nucleation theory (EMLD- DNT) approach to nucleation: A new theory, *J. Phys. Chem. B* **108**, 19831 (2004).
- [20] J. Merikanto, E. Zapadinsky, H. Vehkamäki, and A. Lauri, Origin of the failure of classical nucleation theory: Incorrect description of the smallest clusters, *Phys. Rev. Lett.* **98**, 145702 (2007).

- [21] D. Gebauer and H. Cölfen, Prenucleation clusters and non-classical nucleation, *Nano Today* **6**, 564 (2011).
- [22] S. Prestipino, A. Laio, and E. Tosatti, Systematic improvement of classical nucleation theory, *Phys. Rev. Lett.* **108**, 225701 (2012).
- [23] J. R. Espinosa, C. Vega, C. Valeriani, and E. Sanz, Seeding approach to crystal nucleation, *J. Chem. Phys.* **144**, 034501 (2016).
- [24] G. M. Coli and M. Dijkstra, An artificial neural network reveals the nucleation mechanism of a binary colloidal AB₁₃ crystal, *ACS Nano* **15**, 4335 (2021).
- [25] W. Gispen and M. Dijkstra, Brute-force nucleation rates of hard spheres compared with rare-event methods and classical nucleation theory, *J. Chem. Phys.* **159**, 086101 (2023).
- [26] W. Gispen and M. Dijkstra, Finding the differences: Classical nucleation perspective on homogeneous melting and freezing of hard spheres, *J. Chem. Phys.* **160**, 141102 (2024).
- [27] D. W. Oxtoby, Nucleation of first-order phase transitions, *Acc. Chem. Res.* **31**, 91 (1998).
- [28] P. R. Ten Wolde and D. Frenkel, Homogeneous nucleation and the Ostwald step rule, *Phys. Chem. Chem. Phys.* **1**, 2191 (1999).
- [29] P. M. Piaggi and M. Parrinello, Kinetic polymorphism in molecular crystals using orientational entropy, *Proc. Natl. Acad. Sci. U.S.A.* **115**, 10251 (2018).
- [30] A. E. Van Driessche, N. Van Gerven, P. H. Bomans, R. R. Joosten, H. Friedrich, D. Gil-Carton, N. A. Sommerdijk, and M. Sleutel, Molecular nucleation mechanisms and control strategies for crystal polymorph selection, *Nature (London)* **556**, 89 (2018).
- [31] C. L. Burcham, M. F. Doherty, B. G. Peters, S. L. Price, M. Salvalaglio, S. M. Reutzel-Edens, L. S. Price, R. K. R. Addula, N. Francia, V. Khanna *et al.*, Pharmaceutical digital design: From chemical structure through crystal polymorph to conceptual crystallization process, *Cryst. Growth Design* **24**, 5417 (2024).
- [32] W. Ostwald, Studien über die bildung und umwandlung fester körper: 1. Abhandlung: Übersättigung und überkaltung, *Z. Phys. Chem.* **22**, 289 (1897).
- [33] J. De Yoreo and S. Whitelam, Nucleation in atomic, molecular, and colloidal systems, *MRS Bull.* **41**, 357 (2016).
- [34] B. Sadigh, L. Zepeda-Ruiz, and J. L. Belof, Metastable-solid phase diagrams derived from polymorphic solidification kinetics, *Proc. Natl. Acad. Sci. U.S.A.* **118**, e2017809118 (2021).
- [35] A. Bupathy, D. Frenkel, and S. Sastry, Temperature protocols to guide selective self-assembly of competing structures, *Proc. Natl. Acad. Sci. U.S.A.* **119**, e2119315119 (2022).
- [36] M. Sleutel, J. Lutsko, A. E. Van Driessche, M. A. Durán-Olivencia, and D. Maes, Observing classical nucleation theory at work by monitoring phase transitions with molecular precision, *Nat. Commun.* **5**, 5598 (2014).
- [37] See Supplemental Material at <http://link.aps.org/supplemental/10.1103/PhysRevLett.134.148201>, which includes Refs. [38–43], for a brief description of the models and techniques used, as well as further analysis showing first-neighbor radial profiles for the three polymorphs and ruling out cross-nucleation and the existence of unfavorable surface sites.
- [38] N. Kern and D. Frenkel, Fluid–fluid coexistence in colloidal systems with short-ranged strongly directional attraction, *J. Chem. Phys.* **118**, 9882 (2003).
- [39] F. Smalenburg and F. Sciortino, Liquids more stable than crystals in particles with limited valence and flexible bonds, *Nat. Phys.* **9**, 554 (2013).
- [40] E. G. Noya, I. Zubietta, D. J. Pine, and F. Sciortino, Assembly of clathrates from tetrahedral patchy colloids with narrow patches, *J. Chem. Phys.* **151**, 094502 (2019).
- [41] M. Dijkstra and E. Luijten, From predictive modelling to machine learning and reverse engineering of colloidal self-assembly, *Nat. Mater.* **20**, 762 (2021).
- [42] Zhang, A. S. Keys, T. Chen, and S. C. Glotzer, Self-assembly of patchy particles into diamond structures through molecular mimicry, *Langmuir* **21**, 11547 (2005).
- [43] N. Sorensson and N. Een, Minisat v1. 13-a sat solver with conflict-clause minimization, *SAT* **2005**, 1 (2005).
- [44] A. Jaekel, P. Lill, S. Whitelam, and B. Saccà, Insights into the structure and energy of DNA nanoassemblies, *Molecules* **25**, 5466 (2020).
- [45] Z. Li, Y. Lim, I. Tanriover, W. Zhou, Y. Li, Y. Zhang, K. Aydin, S. C. Glotzer, and C. A. Mirkin, DNA-mediated assembly of au bipyramids into anisotropic light emitting kagome superlattices, *Sci. Adv.* **10**, eadp3756 (2024).
- [46] W. Zhou, Y. Lim, H. Lin, S. Lee, Y. Li, Z. Huang, J. S. Du, B. Lee, S. Wang, A. Sánchez-Iglesias *et al.*, Colloidal quasicrystals engineered with DNA, *Nat. Mater.* **23**, 424 (2024).
- [47] A. Cumberworth, D. Frenkel, and A. Reinhardt, Simulations of DNA-origami self-assembly reveal design-dependent nucleation barriers, *Nano Lett.* **22**, 6916 (2022).
- [48] J. P. Doye, H. Fowler, D. Prešern, J. Bohlin, L. Rovigatti, F. Romano, P. Šulc, C. K. Wong, A. A. Louis, J. S. Schreck *et al.*, The oxDNA coarse-grained model as a tool to simulate DNA origami, in *DNA and RNA Origami: Methods and Protocols* (Springer, New York, 2023), pp. 93–112.
- [49] H. Liu, M. Matthies, J. Russo, L. Rovigatti, R. P. Narayanan, T. Diep, D. McKeen, O. Gang, N. Stephanopoulos, F. Sciortino *et al.*, Inverse design of a pyrochlore lattice of DNA origami through model-driven experiments, *Science* **384**, 776 (2024).
- [50] J. Russo, F. Romano, L. Kroc, F. Sciortino, L. Rovigatti, and P. Šulc, Sat-assembly: A new approach for designing self-assembling systems, *J. Phys. Condens. Matter* **34**, 354002 (2022).
- [51] F. Romano, J. Russo, L. Kroc, and P. Šulc, Designing patchy interactions to self-assemble arbitrary structures, *Phys. Rev. Lett.* **125**, 118003 (2020).
- [52] L. Rovigatti, J. Russo, F. Romano, M. Matthies, L. Kroc, and P. Šulc, A simple solution to the problem of self-assembling cubic diamond crystals, *Nanoscale* **14**, 14268 (2022).
- [53] The number of forms known for a given compound is proportional to the time and money spent in research on that compound.
- [54] P. Virnau and M. Müller, Calculation of free energy through successive umbrella sampling, *J. Chem. Phys.* **120**, 10925 (2004).

- [55] C. Beneduce, F. Sciortino, P. Šulc, and J. Russo, Engineering azeotropy to optimize the self-assembly of colloidal mixtures, *ACS Nano* **17**, 24841 (2023).
- [56] C. Beneduce, D. EP Pinto, P. Šulc, F. Sciortino, and J. Russo, Two-step nucleation in a binary mixture of patchy particles, *J. Chem. Phys.* **158**, 154502 (2023).
- [57] L. Rovigatti, J. Russo, and F. Romano, How to simulate patchy particles, *Eur. Phys. J. E* **41**, 59 (2018).
- [58] B. Chen and J. I. Siepmann, A novel monte carlo algorithm for simulating strongly associating fluids: Applications to water, hydrogen fluoride, and acetic acid, *J. Phys. Chem. B* **104**, 8725 (2000).
- [59] P. J. Steinhardt, D. R. Nelson, and M. Ronchetti, Bond-orientational order in liquids and glasses, *Phys. Rev. B* **28**, 784 (1983).
- [60] P. Rein ten Wolde, M. J. Ruiz-Montero, and D. Frenkel, Numerical calculation of the rate of crystal nucleation in a Lennard-Jones system at moderate undercooling, *J. Chem. Phys.* **104**, 9932 (1996).
- [61] W. Lechner and C. Dellago, Accurate determination of crystal structures based on averaged local bond order parameters, *J. Chem. Phys.* **129**, 114707 (2008).
- [62] C. Desgranges and J. Delhommelle, Crystallization mechanisms for supercooled liquid Xe at high pressure and temperature: Hybrid Monte Carlo molecular simulations, *Phys. Rev. B* **77**, 054201 (2008).
- [63] J. Russo and H. Tanaka, The microscopic pathway to crystallization in supercooled liquids, *Sci. Rep.* **2**, 505 (2012).
- [64] J. Russo and H. Tanaka, Selection mechanism of polymorphs in the crystal nucleation of the Gaussian core model, *Soft Matter* **8**, 4206 (2012).
- [65] J. F. Lutsko and C. Schoonen, A microscopic approach to crystallization: Challenging the classical/non-classical dichotomy, [arXiv:2406.17543](https://arxiv.org/abs/2406.17543).
- [66] S. Whitelam and R. L. Jack, The statistical mechanics of dynamic pathways to self-assembly, *Annu. Rev. Phys. Chem.* **66**, 143 (2015).
- [67] F. Zhang, Nonclassical nucleation pathways in protein crystallization, *J. Phys. Condens. Matter* **29**, 443002 (2017).
- [68] J. Russo and H. Tanaka, Crystal nucleation as the ordering of multiple order parameters, *J. Chem. Phys.* **145**, 211801 (2016).
- [69] D. James, S. Beairsto, C. Hartt, O. Zavalov, I. Saika-Voivod, R. K. Bowles, and P. H. Poole, Phase transitions in fluctuations and their role in two-step nucleation, *J. Chem. Phys.* **150** (2019).
- [70] J. F. Lutsko, How crystals form: A theory of nucleation pathways, *Sci. Adv.* **5**, eaav7399 (2019).
- [71] S. Becker, E. Devijver, R. Molinier, and N. Jakse, Unsupervised topological learning approach of crystal nucleation, *Sci. Rep.* **12**, 3195 (2022).
- [72] C. Schoonen and J. F. Lutsko, Crystal polymorphism induced by surface tension, *Phys. Rev. Lett.* **129**, 246101 (2022).
- [73] W. Gispen, G. M. Coli, R. van Damme, C. P. Royall, and M. Dijkstra, Crystal polymorph selection mechanism of hard spheres hidden in the fluid, *ACS Nano* **17**, 8807 (2023).